Heliyon 9 (2023) e22792

Contents lists available at ScienceDirect

Heliyon

journal homepage: www.cell.com/heliyon

Silicon flower structures by maskless plasma etching

Geng Zhao [a,b,c], Xiaoyan Zhao [d], Haimiao Zhang [d], Ziwei Lian [e], Yongmin Zhao [e], Anjie Ming [e,**], Yuanwei Lin [d,*]

[a] Institute of Solid State Physics, College of Physics and Electronic Science, Shanxi Province Key Laboratory of Microstructure Electromagnetic Functional Materials, Datong University, Datong, 037054, Shanxi Province, China
[b] Department of Physics, Fudan University, Shanghai, 200433, China
[c] Laboratory of Micro-Nano Optoelectronic Materials and Devices, Key Laboratory of Materials for High-Power Laser, Shanghai Institute of Optics and Fine Mechanics, Chinese Academy of Sciences, Shanghai, 201800, China
[d] Department of Semiconductor Etching, NAURA Technology Group Co., Ltd., Beijing, 100176, China
[e] State Key Laboratory of Advanced Materials for Smart Sensing, General Research Institute for Nonferrous Metals, Beijing, 101402, China

ARTICLE INFO

Keywords:
Silicon flower microstructures
Black silicon
Maskless plasma etching
Fluorocarbon gas
Infra-Red absorption

ABSTRACT

Silicon nano/microstructures are widely utilized in the semiconductor industry, and plasma etching is the most prominent method for fabricating silicon nano/microstructures. Among the variety of silicon nano/microstructures, black silicon with light-trapping properties has garnered broad interest from both the scientific and industrial communities. However, the fabrication mechanism of black silicon remains unclear, and the light absorption of black silicon only focuses on the near-infrared region thus far. Herein, we demonstrate that black silicon can be fabricated from individual flower-like silicon microstructures. Using fluorocarbon gases as etchants, silicon flower microstructures have been formed via maskless plasma etching. Black silicon forming from silicon flower microstructures exhibits strong absorption with wavelength from 0.25 μm to 20 μm. The result provides novel insight into the understanding of the plasma etching mechanism in addition to offering further significant practical applications for device manufacturing.

1. Introduction

Silicon nano/microstructures have applications in several fields, such as integrated circuits [1], discrete electronic devices [2], micro-electro-mechanical systems (MEMS) [3], silicon microcavities [4], photonic devices [5], and advanced packaging [6]. Compared with flexible carbon nano/microstructures prepared by the "bottom-up" method [7–9], bulk silicon exhibits higher rigidity, and the "top-down" method is better to be considered for fabricating silicon nano/microstructures. Thus, the dry method which utilizes plasma etching [10,11], and the wet method which utilizes photoelectrochemical etching [12,13] are prominently employed. Although the wet method exhibits a higher throughput, dry method exhibits a better profile performance and is widely applied in the semiconductor industry. Sulfur hexafluoride (SF_6) is typically used as an etchant in dry silicon etching [14,15], and maskless plasma etching technology can reduce the cost of silicon microstructure fabrication because photolithography is expensive and complicated [16–18].

Unlike to obtain smooth surface by etching in usual situation [19], the silicon wafer with light-trapping microstructure on its rough

* Corresponding author.
** Corresponding author.
E-mail addresses: mingaj@bu.edu (A. Ming), yuanweilin@pku.edu.cn (Y. Lin).

https://doi.org/10.1016/j.heliyon.2023.e22792
Received 14 May 2023; Received in revised form 17 October 2023; Accepted 20 November 2023
Available online 22 November 2023

surface, known as “black silicon” [20], has been widely adopted in bactericidal devices [21], solar cells [22–24], and field emission devices [25]. Plasma etching with a gas mixture of SF_6 and oxygen (O_2) is a major technology for obtaining black silicon even without a mask owing to the random formation of micromasks. Other etchants have been investigated by various researchers. However, in most cases, masks are still necessary. Chen et al. employed a reactive ion mixture of hydrogen bromide (HBr) and O_2 to form silicon oxybromide nanodots as masks [26]. Jeong et al. prepared a Langmuir–Blodgett monolayer of silica nanoparticles on silicon substrates, followed by a gas mixture of O_2 and CHF_3 to obtain black silicon [27]. Li et al. fabricated silicon hollow-tip arrays via a metal catalytic wet etching process, where the PS microspheres were utilized as masks [28]. However, the mechanism of black silicon fabrication without masks remains unclear [29]. Furthermore, the optical property of black silicon reported in literature is limited to the near-infrared region [20,28–31].

Herein, we report a novel flower-like silicon microstructure obtained by maskless plasma etching utilizing fluorocarbon gases, such as octafluorocyclobutane (C_4F_8) and carbon tetrafluoride (CF_4), as etchants. The black silicon formed from the silicon flower microstructures exhibits light-trapping property with strong absorption from 0.25 μm to 20 μm. To the best of our knowledge, this is the first report of black silicon absorption close to far-infrared region. Thus, the fabrication of silicon flower structures by maskless plasma etching provides novel insight into the understanding of the plasma etching mechanism in addition to offering further significant practical applications for manufacturing devices, such as photodetectors, solar cells, and field emission devices.

2. Experimental methods

In this work, standard 12-inch *p*-type silicon wafers (resistivity of 1–20 Ω cm) with a single side polished and (100) face upward were commercially purchased. Following the cleaning of silicon wafers by piranha solution, the plasma etching was performed utilizing a NAURA HSE P230 chamber with inductively coupled plasma (ICP) generated by an ICP source power at 13.56 MHz and driven by bias power at 13.56 MHz. Scanning electron microscope (SEM) images of etched silicon wafers were obtained via a Hitachi SU8000. Energy Dispersive X-Ray (EDX) analysis was conducted with EDAX TEAM™ spectrometer equipped in the SEM with a takeoff angle of 35° and an elapsed live-time of 30.0 s, respectively. Optical microscope (OM) characterizations were obtained from an OLYMPUS BX51 M. Atomic force microscope (AFM) characterization was conducted on a Bruker Dimension EDGE using the tapping mode. The dispersed silicon flower sample in ethanol was prepared utilizing a KH-100DB ultrasonic cleaner (Kunshan Hechuang ultrasonic instruments Co., Ltd.). The transmission spectra of the samples were implemented on the PerkinElmer Lambda 900 spectrophotometer (with wavelength range of 0.25–3 μm) and a Nicolet 6700 FTIR spectrometer (with wavelength range of 2.5–20 μm).

3. Results and discussion

The plasma etching of silicon is realized owing to the formation of gaseous silicon tetrafluoride by fluorine free radicals, which can be pumped away from the wafer.

$$Si + x\ F\cdot \rightarrow SiF_x\ (g)$$

Fluorine free radicals are typically generated from SF_6:

$$SF_6 + e^- \rightarrow S_xF_y^+ + S_xF_y\cdot + F\cdot + e^-$$

In addition, fluorocarbon gases can be used to generate fluorine free radicals:

$$C_xF_y + e^- \rightarrow CF_z^+ + CF_z\cdot + F\cdot + e^-$$

The stoichiometric ratio of fluorine in SF_6 is higher than that of C_xF_y (such as C_4F_8 and CF_4), thus, the etch rate is higher with SF_6 as the etchant. However, a higher etch rate may obscure useful information regarding the plasma etching. To reveal the underlying mechanism of black silicon formation, we utilized CF_4 and Ar as the etchant gases in plasma etching (Table 1).

As illustrated in Fig. 1a–c, certain flower-like silicon microstructures with diameter of ~20 μm appear on the wafer surface following etching for a relatively long time (180 min). Cross-sectional SEM image (Fig. 1d) and AFM characterization (Fig. 1e and f) illustrate that the height difference within the silicon flower microstructures is ~5 μm. The silicon flower microstructures demonstrate

Table 1
Comparison of the etching process parameters.

Process parameters	1#	2#
Chuck temperature (°C)	20	20
Chamber pressure (mTorr)	10	5
Center source power (W)	750	1600
Edge source power (W)	750	1800
CF_4 etch gas flow (sccm)	40	–
Ar gas flow (sccm)	80	25
C_4F_8 gas flow (sccm)	–	15
Bias power (W)	100	300
Etch time (min)	Depends on the coverage	

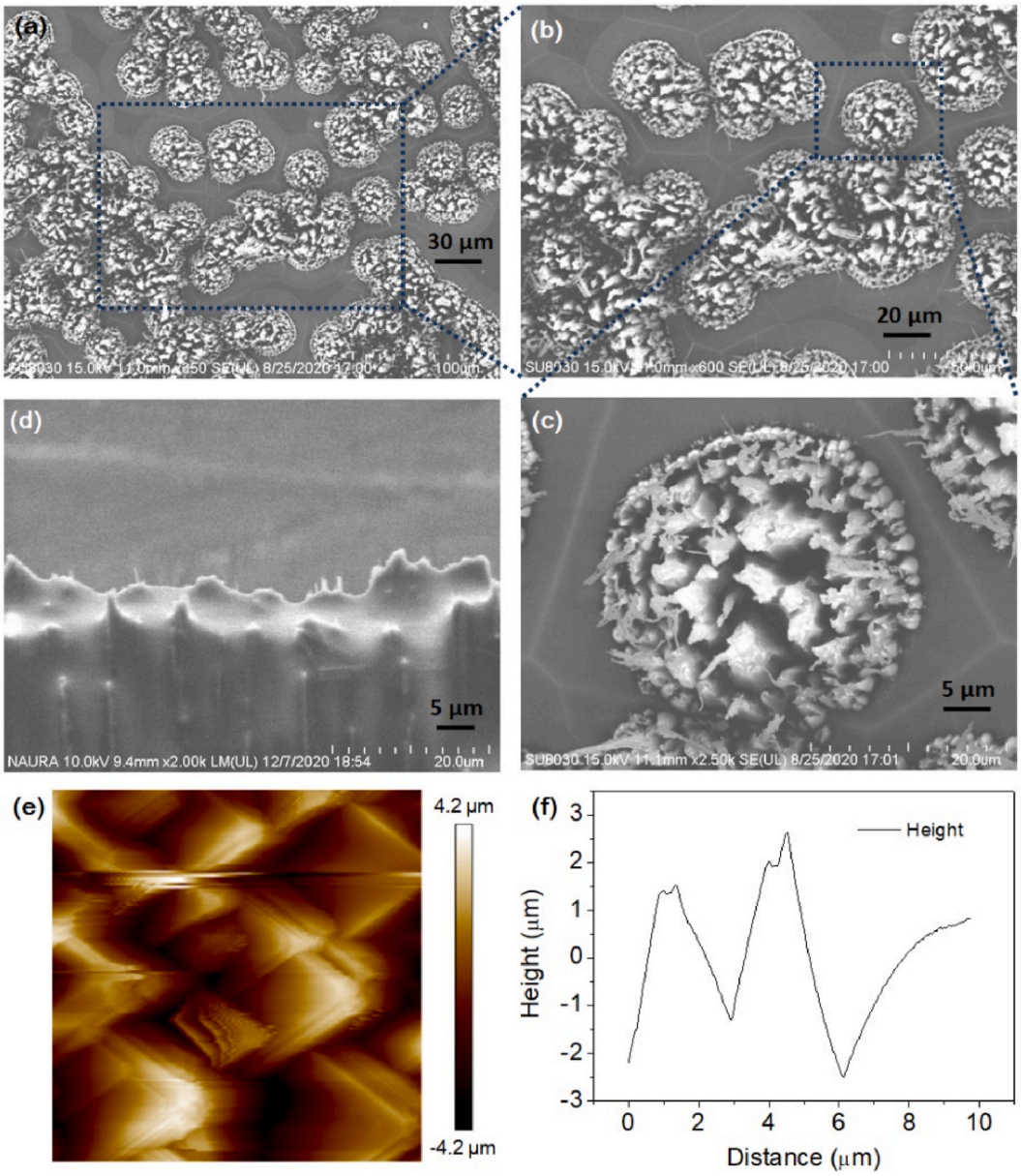

Fig. 1. Characterization of the silicon flower microstructures: (a–c) SEM images of silicon flower microstructures with different magnifications (coverage of ~77.59 %); (d) cross-sectional SEM image of the silicon flower microstructure; (e, f) AFM characterization and height vs. distance curve of the silicon flower microstructure. (For interpretation of the references to colour in this figure legend, the reader is referred to the Web version of this article.)

that mechanism of formation of black silicon is not integral molding but more like the formation of nucleation sites in crystal growth.

When the etching time increases, several needle-like microstructures appear (Fig. 2a). To verify the composition of the flower-like and needle-like microstructures, EDX characterizations were carried out (Fig. 2b–e). The signal of fluorine can be attributed to the fluorine-based etchant, and the appearance of Al element is because the fixture for EDX characterization is made of Al. Thus, the flower-like and needle-like microstructures consist of solely silicon elements.

When the etching time further increases, the silicon flowers are connected to form black silicon (Fig. 3a and b). In addition, the silicon needles become smaller and sharper (Fig. 3c and d). It is worth mentioning that the length of the silicon needles (etch depth) can approach over 50 μm, which provides a nice microstructure for light trapping. EDX characterization demonstrates that the black silicon exhibits no contamination (Fig. 4).

Fig. 5 illustrates the etching-time-dependent coverage of the wafer by silicon flowers. Further, we used a C_4F_8 as the etchant gas and observed that the etch rate (indicated by the growth of the wafer coverage) was slower than that of CF_4 (Fig. 5a). Both higher source

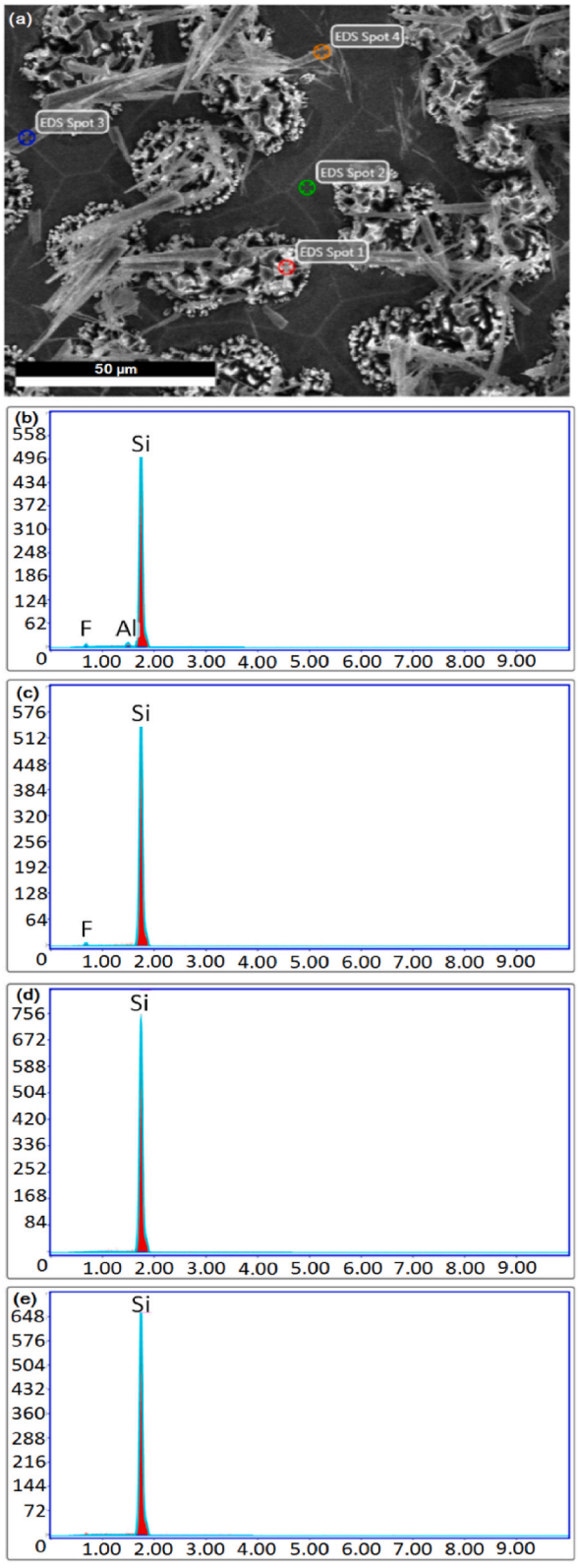

Fig. 2. EDX Characterization of the microstructures on the silicon wafer: (a) SEM image showing the measurement sites; element analysis of the (b) silicon flower microstructures, (c) silicon wafer, and (d, e) silicon needles by EDX. (For interpretation of the references to colour in this figure legend, the reader is referred to the Web version of this article.)

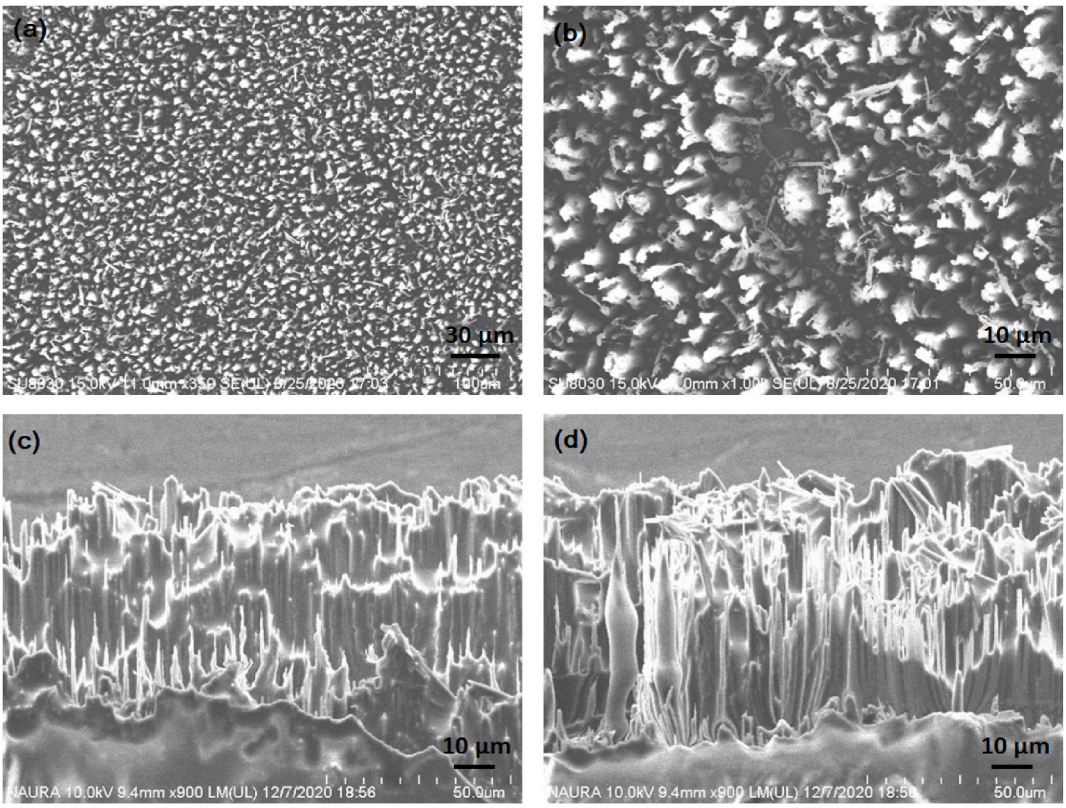

Fig. 3. Characterization of the black silicon formed by silicon flower microstructures: (a, b) SEM images of the black silicon with different magnifications; cross-sectional SEM images of the black silicon at the wafer center (c) and the wafer edge (d).

power and bias power were employed (Table 1). This is because more fluorocarbon free radicals are formed from C_4F_8 than from CF_4, and fluorocarbon free radicals can be further converted to fluorocarbon polymers, which resist plasma etching.

$$n\ CF_z\cdot \rightarrow [CF_2]_n$$

It is noted that this is a maskless method, and the coverage can be tuned by varying etching times. Photolithography is the most expensive process employed in the semiconductor industry. To demonstrate the compatibility of this method with masks, we utilized a metal shadow mask to fabricate black silicon with patterns (Fig. 5b). The etching result exhibited an interface between black and bare silicon (Fig. 5c). The OM images of the black silicon zone illustrate that the silicon flowers coverage is almost 100 %.

Black silicon is an ideal microstructure for trapping lights, and the transmission spectra of the samples were measured on the entire black silicon wafer. Fig. 6a illustrates that the black silicon formed by silicon flower microstructures exhibits a broad absorption from UV–visible to far-infrared, whereas conventional literature only focus on the UV–visible and near-infrared region [20,28–31]. To demonstrate the light trapping mechanism, the wafer containing black silicon was ultrasonically soaked in ethanol, and the suspension with dispersed silicon microstructures exhibited no obvious absorption (Fig. 6b). This illustrates that the silicon microstructures (such as flowers and needles that forming deep holes) in solid state are the origin of the light-trapping function of black silicon. Comparison between black and bare silicon further demonstrates that microstructures matter in the mechanism of its light-trapping property. Fig. 6c and d illustrate that the transmittance of black silicon is close to 0 in the wavelength range of 0.25–10 μm. The transmittance starts to increase from 10 μm and approaches ~10 % at 20 μm. For comparison, the transmittance of bare silicon is larger than 50 % in the wavelength range of 2.5–20 μm, except for some special absorption bands. Though the decrease of transmittance in black silicon compared with bare silicon may be ascribed to two reasons: a) increase of reflectance or b) increase of absorption, from the optical microscope images (such as Fig. 5c), we can see the reflectance of black silicon is weaker than that of bare silicon, at least for the visible region. Besides, the literatures [20,24,30] have demonstrated the reflectance of bare silicon is stronger than that of black silicon with similar microstructures reported in this work. In addition, it is a common sense that the reflection will be stronger if the surface is smoother, whereas the black silicon has a rough surface. Thus, the decrease of transmittance in black silicon compared with bare silicon shown in this work can only be explained by the increase of absorption. The results indicate that black silicon formed from silicon flowers exhibits a higher absorption than that of bare silicon in UV–visible–infrared region, which makes it a potential candidate for fabrication of optoelectronic devices, such as photodetectors and solar cells.

To further discuss the maskless plasma etching mechanism forming silicon flower and black silicon, it is reasonable to consider more about the reactive details of the plasma etching process. In reactive chamber, the etching gas (CF_4 or C_4F_8) can be ignited by RF

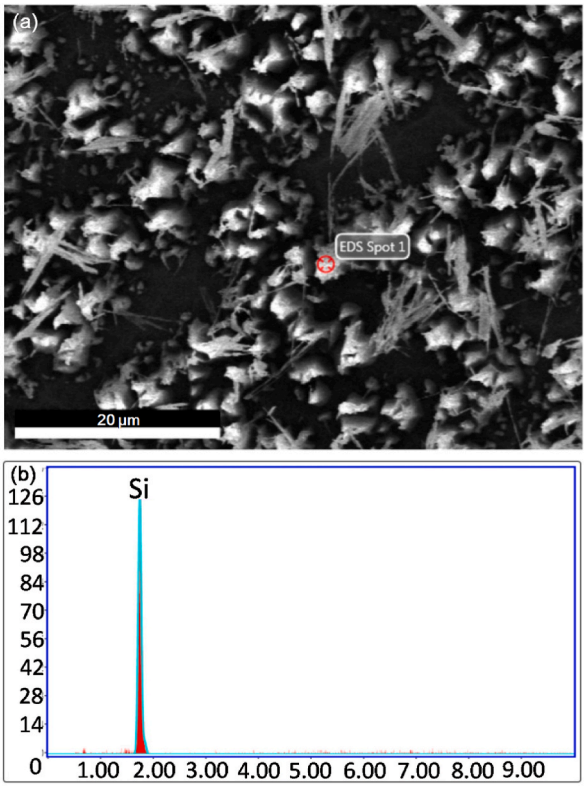

Fig. 4. EDX Characterization of the black silicon formed by silicon flower microstructures: (a) SEM image showing the measurement site; (b) element analysis by EDX. (For interpretation of the references to colour in this figure legend, the reader is referred to the Web version of this article.)

coil forming anion (CF_n^+ or $C_mF_n^+$) and free radicals ($CF_2\cdot$ and $F\cdot$). It is noted that C_4F_8 has a stronger ability to generate $CF_2\cdot$ free radical than that of CF_4, which can explain why it takes more time to have a full coverage of black silicon on the wafer when C_4F_8 is used as etching gas (Fig. 5a).

$$CF_4 + e^- \rightarrow CF_n^+ + CF_2\cdot + F\cdot + e^-$$

$$C_4F_8 + e^- \rightarrow C_mF_n^+ + CF_2\cdot + F\cdot + e^-$$

Then, $CF_2\cdot$ free radical has a strong tendency to form fluorocarbon polymer $[CF_2]_n$. Due to the high reactive rate, the fluorocarbon polymer layer is not uniform. This is also the reason why the silicon flowers formed are randomly distributed.

$$nCF_2\cdot \rightarrow [CF_2]_n$$

With the help of the acceleration by bias power, anion (CF_n^+ or $C_mF_n^+$) has a physical bombardment effect on the wafer. At the wafer area with thinner fluorocarbon polymer layer, the physical bombardment on the fluorocarbon polymer will expose the silicon wafer underneath. Otherwise, the silicon wafer will be still covered by a thin layer of fluorocarbon polymer, and that is why it is a maksless process. Then, the silicon wafer is etched by $F\cdot$ free radical.

$$Si + x\ F\cdot \rightarrow SiF_x\ (g)$$

It is worth mentioning that this is an exothermic reaction, and high temperature hampers the occurring of the fluorocarbon polymer formation reaction. Thus, the area of the silicon wafer exposed to the plasma has excessive etching effect, which will form silicon flower structure, whereas the area covered by a thin layer of fluorocarbon polymer will be still flat area without rough surface. With the increase of the etching time, the silicon flowers will join together to take up all the wafer area to fully form the black silicon structure. Due to the higher aspect ratio of the needle structure formed on the black silicon surface, the light absorption performance of the black silicon reported in this work is improved compared with the results in the literatures. The mechanism mentioned above can be summarized in Fig. 7. It is noted that the process is a continuous one, though in Fig. 7 the process is separated by several steps to make it more readable.

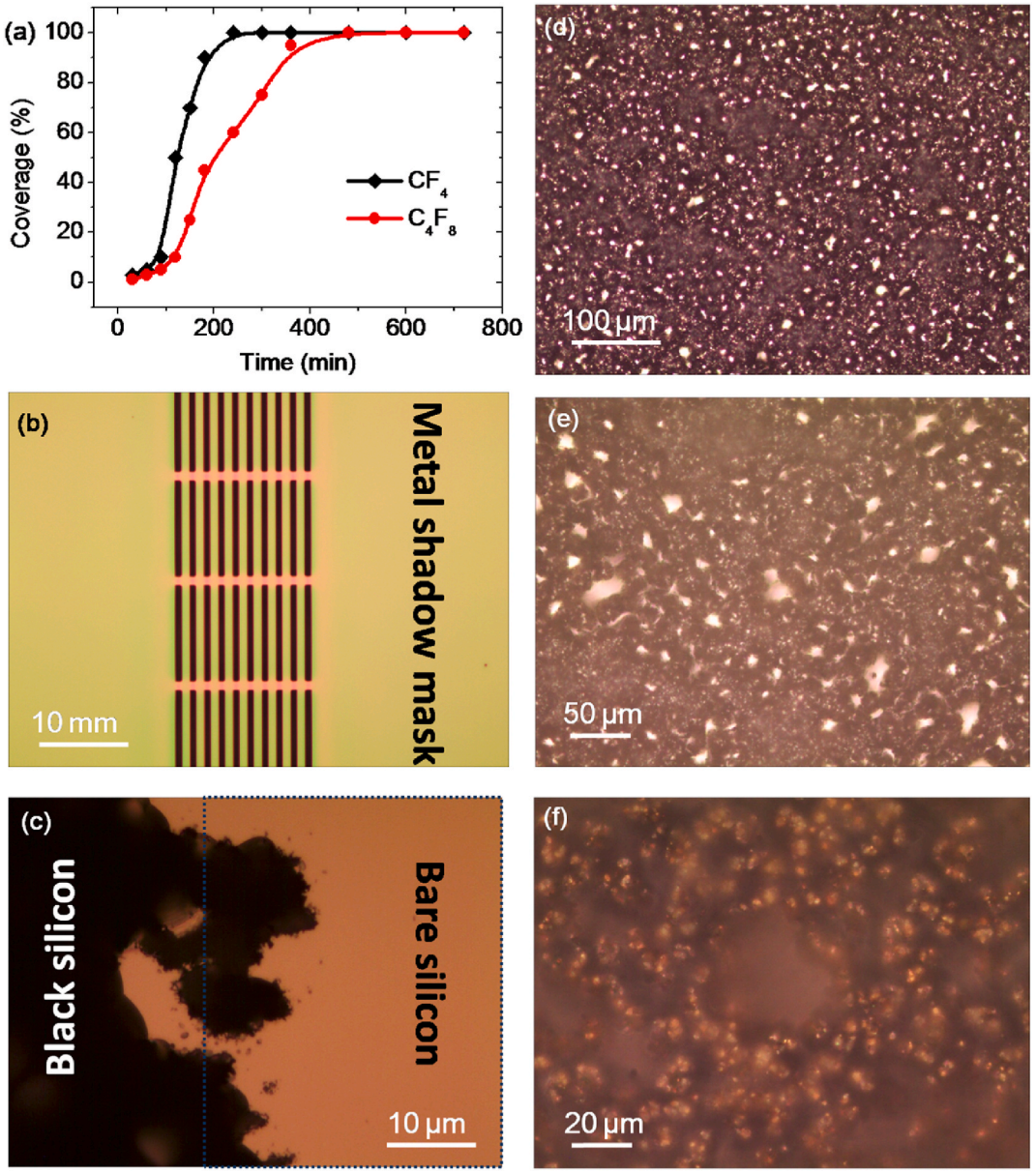

Fig. 5. Further characterizations of the silicon flower microstructures: (a) etchant and etching time-dependent silicon flower coverage; (b) OM image of the metal shadow mask; (c) OM image showing the interface of the black silicon and bare silicon; (d–f) OM images of the black silicon formed by silicon flower microstructures. (For interpretation of the references to colour in this figure legend, the reader is referred to the Web version of this article.)

4. Conclusion

In summary, we demonstrated that flower-like silicon microstructures can be formed by maskless plasma etching using fluorocarbon gases as etchants. The black silicon formed by the silicon flower microstructures exhibits strong absorption in a wide range from 0.25 μm to 20 μm. In particular, its ability to trap light close to the far-infrared region makes it possible to fabricate mid-infrared and even far-infrared photodetectors. The silicon microstructure dominated by gas types provides a novel perspective for the plasma etching mechanism, and the investigation of UV–visible–infrared absorption of black silicon consisting of silicon flowers is significant for optical device fabrication/manufacturing in both the scientific and industrial communities.

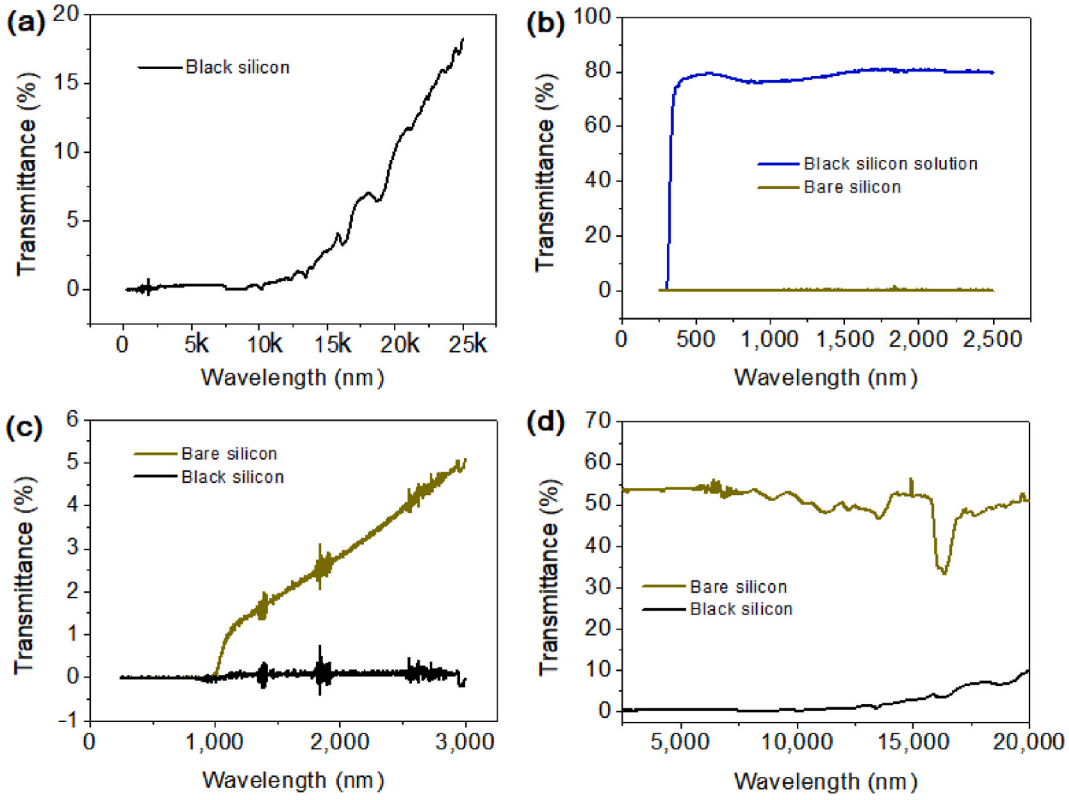

Fig. 6. Transmittance characterizations: (a) Transmittance characterizations of the black silicon formed by silicon flower microstructures with wavelength range of 0.25–25 μm; (b) comparison of the transmittance of the black silicon ultrasonically dispersed in ethanol and black silicon wafer; comparison of the transmittance of the black silicon wafer and bare silicon wafer at wavelength ranges of (c) 250–3000 nm and (d) 2500–20000 nm. (For interpretation of the references to colour in this figure legend, the reader is referred to the Web version of this article.)

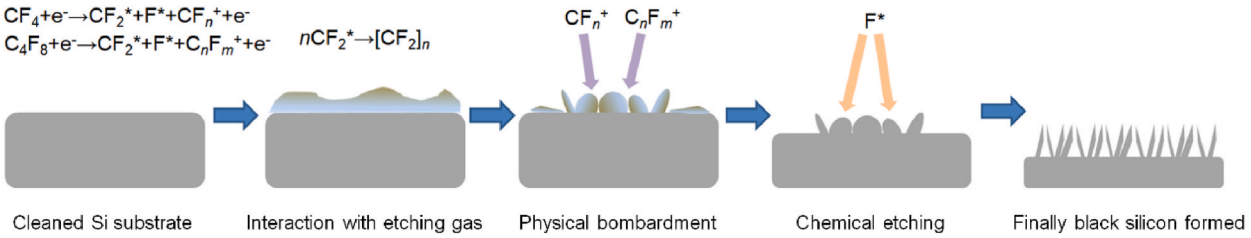

Fig. 7. Schematic illustration of the silicon flower and black silicon formation mechanism by maskless plasma etching. (For interpretation of the references to colour in this figure legend, the reader is referred to the Web version of this article.)

Data availability statement

Data will be made available on request.

CRediT authorship contribution statement

Geng Zhao: Data curation, Formal analysis, Funding acquisition, Investigation, Writing – original draft. **Xiaoyan Zhao:** Data curation, Formal analysis, Investigation. **Haimiao Zhang:** Data curation, Formal analysis, Investigation. **Ziwei Lian:** Data curation, Formal analysis, Investigation. **Yongmin Zhao:** Data curation, Formal analysis, Investigation. **Anjie Ming:** Conceptualization, Funding acquisition, Writing – review & editing. **Yuanwei Lin:** Conceptualization, Data curation, Formal analysis, Investigation, Validation, Writing – original draft, Writing – review & editing.

Declaration of competing interest

The authors declare that they have no known competing financial interests or personal relationships that could have appeared to influence the work reported in this paper.

Acknowledgements

This work was financially supported by National Key Research and Development Project (2019YFB2005705), National Natural Science Foundation of China (61874137), the Science and Technology Innovation Project of Shanxi Colleges and Universities (Grant No. 2023L268) and Shanxi Datong University Project (No.2022Q23). The authors thank Ms. Jing Liu and Ms. Tingting Li for SEM measurement. Yuanwei Lin thanks Dr. Ming Zhuo and Dr. Gangli Chen for beneficial discussion for this work.

References

[1] D.X. Dai, D. Liang, P. Cheben, Photonics Research, NGSP1-NGSP3 10 (2022).
[2] X. Luo, T.F. Lei, Y.G. Wang, G.L. Yao, Y.H. Jiang, K. Zhou, P. Wang, Z.Y. Zhang, J. Fan, Q. Wang, R. Ge, B. Zhang, Z. Li, F. Udrea, IEEE Trans. Electron Devices 59 (2012) 504–509.
[3] P. Norlin, M. Kindlundh, A. Mouroux, K. Yoshida, U.G. Hofmann, J. Micromech. Microeng. 12 (2002) 414–419.
[4] H.L. Han, H. Li, L.X. You, X.P. Liu, Chin. Opt Lett. 20 (2022), 111301.
[5] L.T. Feng, M. Zhang, J.W. Wang, X.Q. Zhou, X.G. Qiang, G. Guo, X.F. Ren, Photon. Res. 10 (2022) A135–A153.
[6] Y. Lin, R. Yuan, C. Zhou, Z. Dong, Z. Su, H. Zhang, Z. Chen, Y. Li, C. Wang, Nanotechnology 31 (2020), 315301.
[7] Y. Lin, X. Guo, Small 11 (2015) 2856–2861.
[8] Y. Lin, G. Lin, B. Sun, X. Guo, Adv. Funct. Mater. 28 (2018), 1705589.
[9] S. Chen, D.M. Koshy, Y. Tsao, R. Pfattner, X. Yan, D. Feng, Z. Bao, J. Am. Chem. Soc. 140 (2018) 10297–10304.
[10] C.P. D'Emic, J. Vac. Sci. Technol. B 10 (1992) 1105–1110.
[11] Y. Cui, S. Jian, C. Chen, Y. Lin, Z. Su, H. Zhang, R. Yuan, Z. Chen, Z. Dong, L. Li, Q. Xie, C. Wang, S. Guo, X. Wang, D. Yu, D. Li, J. Micromech. Microeng. 29 (2019), 105010.
[12] T. Geppert, S.L. Schweizer, U. Gösele, R.B. Wehrspohn, Appl. Phys. A 84 (2006) 237–242.
[13] X. Li, H.S. Seo, H.D. Um, S.W. Jee, Y.W. Cho, B. Yoo, J.H. Lee, Electrochim. Acta 54 (2009) 6978–6982.
[14] M.A. Blauw, T. Zijlstra, R.A. Bakker, E. van der Drift, J. Vac. Sci. Technol. B 18 (2000) 3453.
[15] A. Herrick, A.J. Perry, R.W. Boswell, J. Vac. Sci. Technol. A 21 (2003) 955–966.
[16] T. Hamada, Mat. Sci. Semicon. Proc. 66 (2017) 212–214.
[17] M. Mansoor, I. Haneef, A. De Luca, J. Coull, F. Udrea, J. Micromech. Microeng. 28 (2018), 085013.
[18] C. Zhou, J. Dong, B. Zhang, B. Xiao, W. Jie, Y. Xu, Superlattice. Microst. 137 (2020), 106353.
[19] Z. Dong, Y. Lin, Mat. Sci. Semicon. Proc. 105 (2020), 104681.
[20] L.L. Ma, Y.C. Zhou, N. Jiang, X. Lu, J. Shao, W. Lu, J. Ge, X.M. Ding, X.Y. Hou, Appl. Phys. Lett. 88 (2006), 171907.
[21] E.P. Ivanova, J. Hasan, H.K. Webb, G. Gervinskas, S. Juodkazis, V.K. Truong, A.H. Wu, R.N. Lamb, V.A. Baulin, G.S. Watson, J.A. Watson, D.E. Mainwaring, R. J. Crawford, Nat. Commun. 4 (2013) 2838.
[22] H.-C. Yuan, V.E. Yost, M.R. Page, P. Stradins, D.L. Meier, H.M. Branz, Appl. Phys. Lett. 95 (2009), 123501.
[23] J. Oh, H.C. Yuan, H.M. Branz, Nat. Nanotechnol. 7 (2012) 743–748.
[24] H. Savin, P. Repo, G. von Gastrow, P. Ortega, E. Calle, M. Garín, R. Alcubilla, Nat. Nanotechnol. 10 (2015) 624–629.
[25] P. Hoyer, M. Theuer, R. Beigang, E.B. Kley, Appl. Phys. Lett. 93 (2008), 091106.
[26] Y. Chen, Z. Xu, M.R. Gartia, D. Whitlock, Y. Lian, G.L. Liu, ACS Nano 5 (2011) 8002–8012.
[27] S. Jeong, M.D. McGehee, Y. Cui, Nat. Commun. 4 (2013) 2950.
[28] Y. Li, J. Zhang, S. Zhu, H. Dong, Z. Wang, Z. Sun, J. Guo, B. Yang, J. Mater. Chem. 19 (2009) 1806–1810.
[29] M. Otto, M. Algasinger, H. Branz, B. Gesemann, T. Gimpel, K. Füchsel, T. Käsebier, S. Kontermann, S. Koynov, X. Li, V. Naumann, J. Oh, A.N. Sprafke, J. Ziegler, M. Zilk, R.B. Wehrspohn, Adv. Optical Mater. 3 (2015) 147–164.
[30] H.M. Branz, V.E. Yost, S. Ward, K.M. Jones, B. To, P. Stradins, Appl. Phys. Lett. 94 (2009), 231121.
[31] X. Liu, P.R. Coxon, M. Peters, B. Hoex, J.M. Cole, D.J. Fray, Energy Environ. Sci. 7 (2014) 3223–3263.